ARMY RESEARCH LABORATORY

Design of a Five-Axis Load Cell for Submerged Wing Testing in an Oil Tank

by John Gerdes

ARL-TR-5843 **December 2011**

NOTICES

Disclaimers

The findings in this report are not to be construed as an official Department of the Army position unless so designated by other authorized documents.

Citation of manufacturer's or trade names does not constitute an official endorsement or approval of the use thereof.

Destroy this report when it is no longer needed. Do not return it to the originator.

Army Research Laboratory
Aberdeen Proving Ground, MD 21005-5066

ARL-TR-5843 **December 2011**

Design of a Five-Axis Load Cell for Submerged Wing Testing in an Oil Tank

John Gerdes
Vehicle Technology Directorate, ARL

REPORT DOCUMENTATION PAGE	*Form Approved OMB No. 0704-0188*

1. REPORT DATE *(DD-MM-YYYY)*	2. REPORT TYPE	3. DATES COVERED (From - To)
December 2011	Final	1 March 2011 – 19 May 2011

4. TITLE AND SUBTITLE
Design of a Five-Axis Load Cell for Submerged Wing Testing in an Oil Tank

5a. CONTRACT NUMBER

5b. GRANT NUMBER

5c. PROGRAM ELEMENT NUMBER

6. AUTHOR(S)
John Gerdes

5d. PROJECT NUMBER
W813LT-1139-7045

5e. TASK NUMBER

5f. WORK UNIT NUMBER

7. PERFORMING ORGANIZATION NAME(S) AND ADDRESS(ES)
U.S. Army Research Laboratory
ATTN: RDRL-VTV
Aberdeen Proving Ground, MD 21005-5066

8. PERFORMING ORGANIZATION REPORT NUMBER
ARL-TR-5843

9. SPONSORING/MONITORING AGENCY NAME(S) AND ADDRESS(ES)

10. SPONSOR/MONITOR'S ACRONYM(S)

11. SPONSOR/MONITOR'S REPORT NUMBER(S)

12. DISTRIBUTION/AVAILABILITY STATEMENT
Approved for public release; distribution is unlimited.

13. SUPPLEMENTARY NOTES

14. ABSTRACT
The design of a load cell utilizing the bending beam principle is presented. The load cell measures the forces and moments created by a flapping wing submerged in an oil tank. The design process is described starting with an overview of the design methodology and the conceptual design. The functional and geometric constraints are then identified. Performance requirements are used to optimize the load cell geometry and detail the conceptual design. The electrical circuit design is described in detail, including the design of the bridge circuits used, gauge placement, and corrections applied to account for thermal, drift, and zero loading errors. Finite-element simulations are presented to justify the locations of the gauges on the load cell. The manufacturing and installation process is described, as well as required future work including calibration and testing of the load cell.

15. SUBJECT TERMS
load, cell, wing, oil tank

16. SECURITY CLASSIFICATION OF:			17. LIMITATION OF ABSTRACT	18. NUMBER OF PAGES	19a. NAME OF RESPONSIBLE PERSON
a. REPORT	b. ABSTRACT	c. THIS PAGE			John Gerdes
Unclassified	Unclassified	Unclassified	UU	30	19b. TELEPHONE NUMBER (*Include area code*) 410-278-8735

Standard Form 298 (Rev. 8/98)
Prescribed by ANSI Std. Z39.18

Contents

List of Figures

List of Tables

INTENTIONALLY LEFT BLANK.

1. Introduction

Consumers in a variety of fields frequently need to measure forces and moments generated by some application of interest. As such, load cells have become ubiquitous in today's world, with wide-ranging applications such as commercial, industrial, research, medical, and transportation, etc. Load cells are defined as transducers that convert forces imposed on their structure into measurable electrical signals. Researchers have studied load cells quite substantially over the years, resulting in a large body of data regarding the mechanical and electrical design, calibration procedures, and manufacturing techniques (*1–10*).

Load cells can use a variety of techniques to convert forces into electrical signals; however, the most common approach is the use of strain gauges. Typically, forces are transferred to the load cell through a mechanical connection to the body of interest. The forces transmitted will induce a strain in the material of the load cell which will transfer to the strain gauges, resulting in a change in their resistance. Voltage is then measured through the output of a Wheatstone bridge circuit and sensed using an amplifier, signal conditioner, and data acquisition system. Proper positioning of the gauges, along with good circuit design, allow for a variety of desired measurement properties including increased measurement sensitivity, cancellation of thermal effects, and reduced nonlinearity, making the strain gauge-based load cell an attractive option for force measurement.

While there are many configurations available to the consumer from commercial vendors, these options tend to be expensive if multiple axes of measurement are desired. Furthermore, due to the wide range of potential loading scenarios and configurations, it is not always ideal to use commercial off-the-shelf (COTS) devices. Therefore, many researchers build their own custom sensing devices to provide an inexpensive yet accurate solution.

Customized load cells assure the design is considering the following:

- Measurement of highly specific force and moment magnitudes by a discrete range of COTS devices generally results in some amount of compromise on measurement resolution or range.
- Dynamic systems subject to one or many modes of vibration must be matched to a load cell with natural frequencies well outside the expected range of excitation.
- Systems with unusual external factors including large temperature shifts, potential for submersion in liquids, or unconventional mounting configurations may prevent the use of COTS devices or invalidate calibrations.

- COTS devices tend to come in a limited number of shapes and sizes for a given measurement range. Given a preexisting system, significant effort may be required to integrate a load cell lacking a convenient footprint.
- Custom-built multiaxis commercial load cells can cost thousands of dollars, which can be an inappropriate expenditure, especially for projects that are notional or still under development.

We present a five-axis load cell used for submerged wing testing in a low Reynolds number oil tank. By flapping a large wing slowly through viscous oil, the aerodynamics of rapidly flapping tiny wings in air can be simulated (*11*). Such an arrangement allows more manageable test conditions that are Reynolds scaled to provide insight into the aerodynamic behavior of very small wings, which prove to be experimentally difficult to work with. This load cell will be attached to the end of a drive mechanism that will flap the wing in two degrees of rotation freedom—flap and pitch. The load cell is constructed as a cantilever beam instrumented with piezoresistor-type strain gauges and will operate while submerged in mineral oil.

We also present a procedure that describes the entire design process from start to finish. Engineering aspects considered include identification of desired measurement properties, geometric and functional constraints, and electrical system functionality. The design process will seek to optimize the design of the load cell with respect to the engineering parameters while also satisfying constraints. Additionally, nondesign aspects of importance to the load cell will be discussed, including calibration procedures and manufacturing techniques.

2. Oil Tank Details

A unique set of requirements arises for this load cell from the intended oil tank application. The general functionality is described in Dickinson et al. (*11*); however, the current tank uses only one wing instead of a pair flapping in tandem. The load cell is required as a structural support to drive the flapping of the wing, while also sensing forces arising from interacting with the oil. Therefore, a cantilever beam is used to connect the wing to the driving mechanism. The base of the cantilever is mounted inside a gearbox using a pair of ball bearings and is driven by stepper motors to provide the desired motions for testing (figure 1). The wing under test is mounted to the end of the load cell and must be easily removed for testing a variety of wing styles. The system is able to drive two degrees of freedom, labeled flap and pitch. Shaft encoders provide position feedback; when coupled with the stepper motors and control software, these encoders allow precise control of the wings' motion throughout the flapping range.

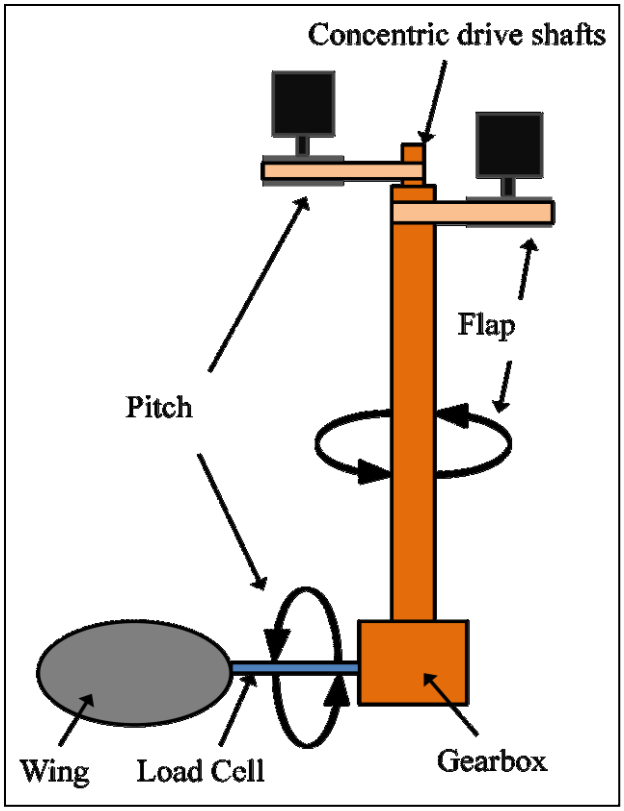

Figure 1. Functional layout of wing flapping system.

3. Conceptual Design

To begin the design process for the load cell, a plan was created to consider the important factors that would impact system performance. Necessary considerations included the mechanical properties of the system, the electrical design, and the interaction with the oil tank system. A general view of the design process is summarized in figure 2.

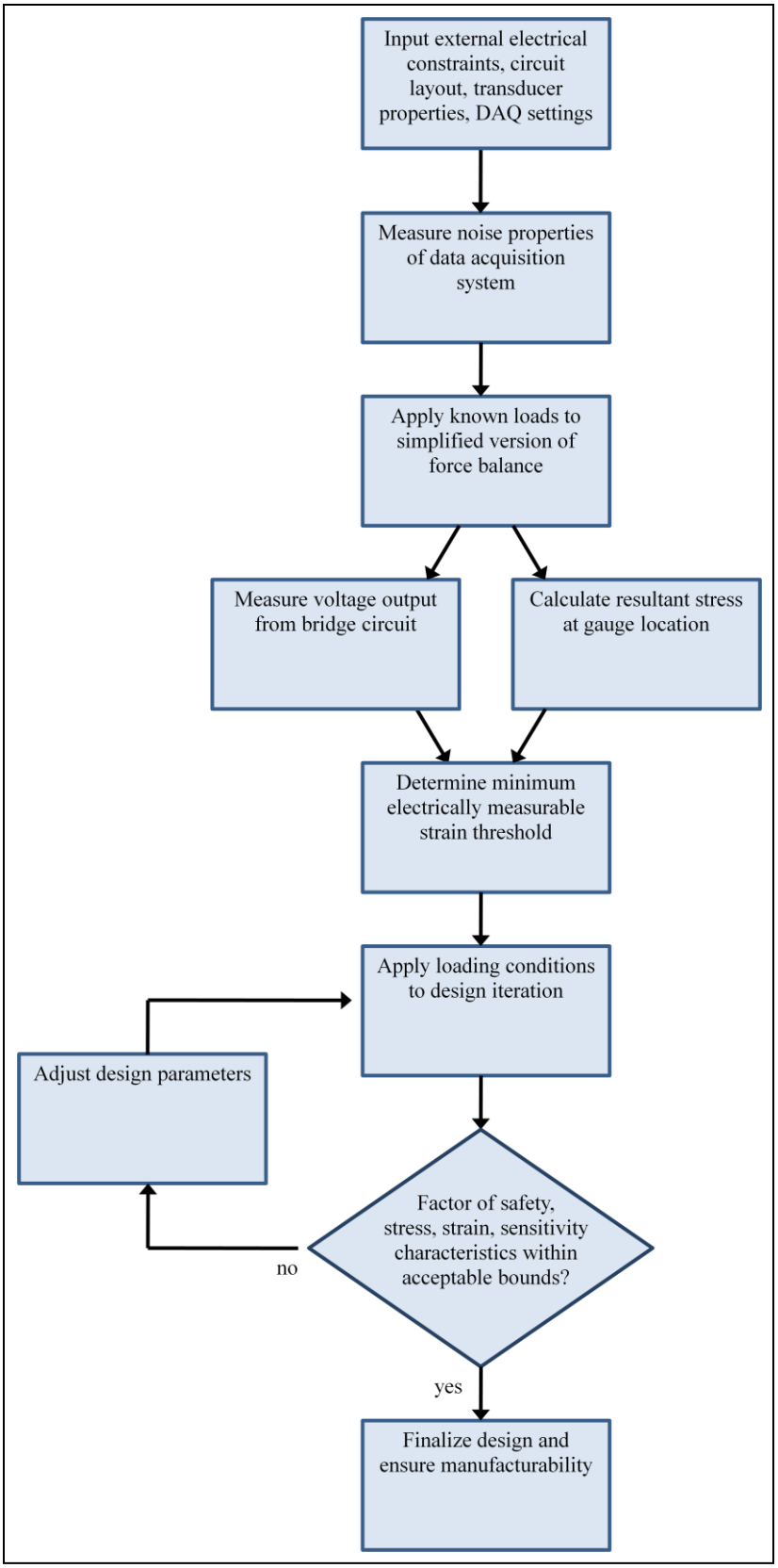

Figure 2. Flow chart of design process.

Some of the geometry of the load cell is prescribed by the design of the oil tank system, thus reducing the number of variables. The driving mechanism is constructed with a pair of integrated ball bearings that hold the load cell in place. This constrains the diameter of the clamped end of the beam used. Since the bearings are integrated into the structure of the driving mechanism, their separation distance is fixed. The length of the load cell was constrained because the root of the wing had to be kept close to the axis of rotation to preserve a flapping motion that would mimic biological sources, as well as to prevent oil flow interactions with the walls of the tank. Due to the required axes of motion to be measured, it was desirable to choose a symmetric cross section. Finally, due to the known interface geometry of multiple preconstructed wings to be tested, the geometry required at the free end of the beam was known. The design concept is shown in figure 3, with the constrained dimensions listed in table 1.

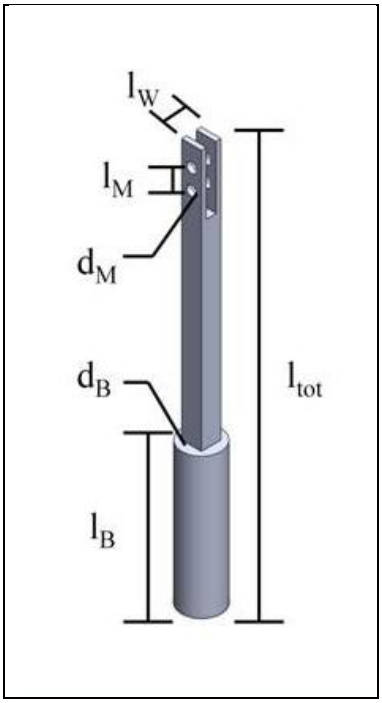

Figure 3. Conceptual design with constrained dimensions.

Table 1. Geometric constraints.

Value	Unit	Description
$\mathbf{l_M}$ = 0.250	Inch	Separation of wing mounting holes
$\mathbf{d_M}$ = 0.125	Inch	Diameter of mounting hardware used for wing mounting
$\mathbf{d_B}$ = 0.500	Inch	Diameter of spar portion mounted inside ball bearings
$\mathbf{l_B}$ > 4.000	Inch	Separation of ball bearings used to mount spar in flapping mechanism
$\mathbf{l_W}$ > 0.125	Inch	Maximum wing thickness
$\mathbf{l_{tot}}$ = 6.000	Inch	Length of spar required to provide proper wing flapping dynamics

4. Sensor Type and Layout

With the general design concept established, it was then necessary to select a method of converting forces imposed on the structure of the load cell to measurable electrical signals. The common technique of using a wheatstone bridge with strain-varying resistors in each of the four arms was chosen due to the wide range of guidance available in implementing such a system (*12–21*).

Piezoresistors were chosen instead of the typical foil-backed strain gauges to provide increased sensitivity (figure 4). Increased sensitivity was needed because large forces are encountered during installation into the flapping mechanism. Piezoresistors allowed the load cell to be designed with an increased margin of safety while still providing acceptable measurement sensitivity and reducing the chance of accidental destruction of the load cell from plastic deformation during assembly. A drawback of piezoresistors is that they are much more susceptible to errors due to thermal effects and material mismatches with the strained part. These issues are discussed in greater detail in section 5.

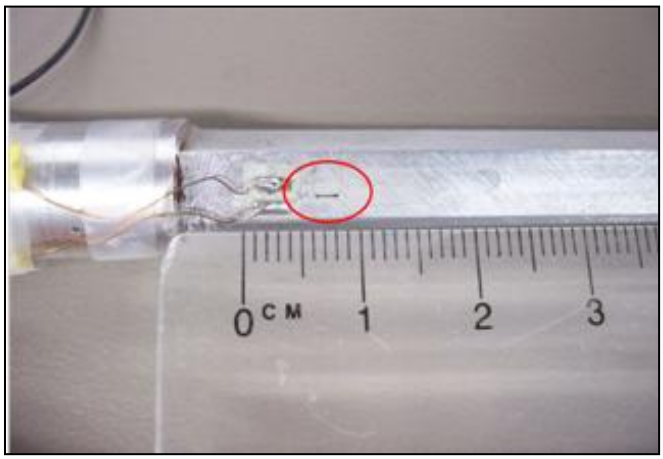

Figure 4. Piezoresistor size photo.

Due to the requirement to measure moments generated during the flapping motion, two bridges must be used along each of the bending axes, separated by a known distance (figure 5). During calibration, known masses are applied to the load cell. Since the gauges farther from the applied load will experience a linearly greater bending moment, there is an expected scaling factor between the front and rear bridges based on the separation distance. Conversely, an applied pitching moment will create the same level of stress in both bridges, regardless of separation distance. Therefore, appropriate scaling factors are determined and allow the separation of the two modes of loading in both bending axes.

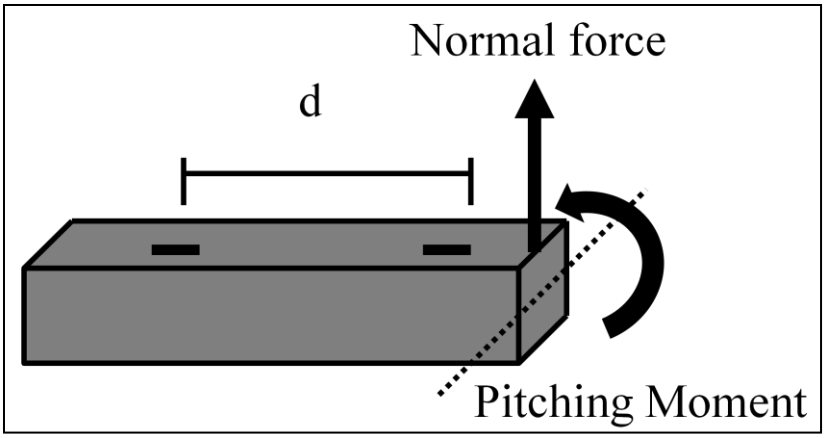

Figure 5. Force/moment separation principle.

Slots were added to the beam to alter the strain field generated by applied loading. Slotting the load cell had multiple effects. The most obvious result was that bending strains were increased relative to a given loading magnitude, increasing sensitivity to lift and thrust measurements. Similarly, slots increased the sensitivity to the torsional load. While this is advantageous for measurement purposes, it also means that permanent damage to the load cell during handling and installation is more likely. The second effect was the presence of a new stress field in the slot areas in response to axial torsion loads. With a slot added, the strain field exhibited alternating fields of tension and compression on each face. The details of the circuit design will be discussed in greater detail in section 6.

5. Optimization of Load Cell Geometry

To guarantee proper operation of the load cell, it was necessary to ensure that expected loads would provide clearly measurable signals while not exceeding the limits imposed by the material properties of the beam or the geometric constraints imposed in figure 3. The magnitude of forces and moments to be measured by the load cell were estimated based on Reynold's number scaling techniques with the coordinate system in figure 6. The loading scenarios of table 2 were designed to capture a wide range of expected loading conditions for currently constructed wings to be tested and represent some of the worst-case scenarios of combined loading.

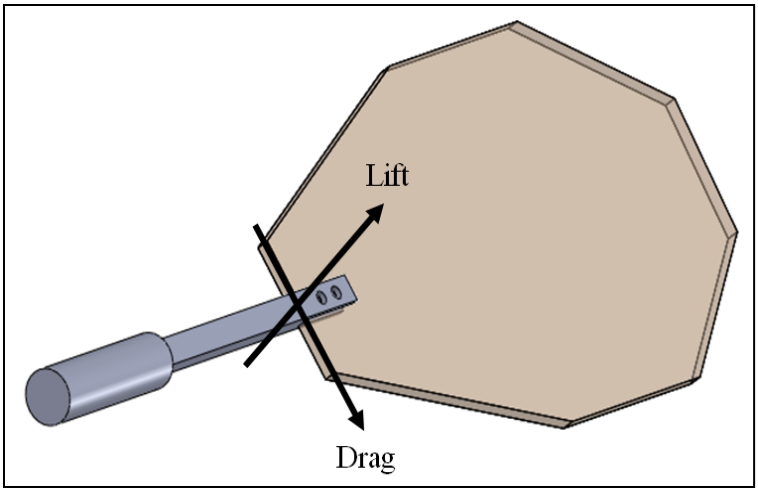

Figure 6. Load cell with mounted test specimen showing coordinate system.

Table 2. Loading scenarios for FEA testing.

X (Extension)		**Y (Drag Bending)**		**Z (Lift Bending)**	
F (N)	**M (N-m)**	**F (N)**	**M (N-m)**	**F (N)**	**M (N-m)**
0.5	±0.0036	0.5	±0.0036	0.5	±0.0036
0	±0.0036	0.5	±0.0036	0.5	±0.0036
0.5	0	0.5	±0.0036	0.5	±0.0036
0	±0.0036	0	0	0	0

Given the constraints on geometry, the primary means of tuning the stiffness of the beam to match the loading conditions was to alter the slot sizes along the beam, thus reducing bending and torsional stiffness. To determine the proper sizing of the slots in the beam, a target stress and corresponding strain magnitude was needed to ensure good quality data that was not being lost in the noise inherent to the data acquisition system. Due to the presence of lead wires, a power supply, an amplifier, and a filter rack, there were a number of possible sources for noise to infiltrate the data. In addition to these hardware components, there were also environmental factors such as fluorescent lights, ground loops in the electrical supply, and other factors contributing to the noise present in the signal. While a variable resistor has infinite resolution from a theoretical standpoint, these noise sources dictate that a finite value be chosen to sufficiently differentiate the desired signal from noise.

Determination of the stress level required for clear measurement was conducted as follows. First, a simplified version of the load cell was constructed. This consisted of a rectangular cross-section beam instrumented with a single piezoresistor of the type to be used in the final part.

This beam was clamped and subjected to a number of calibrated loads. Using beam theory and finite-element analysis (FEA), the stress arising in the beam was easily determined as a linear function of the applied load. With this knowledge, the magnitude of loading applied to the beam was then decreased steadily until it was no longer possible to distinguish the measured voltage response from the noise in the data acquisition system. This amount of stress was then used to calculate a corresponding strain that was present on the beam at the location of the piezoresistor.

Experimental results revealed that approximately 0.25 με was the lower limit of measurability. Below this point, measurements became erratic and difficult to distinguish from noise present in the system.

Since the load cell uses a full bridge configuration, the required voltage threshold is achieved by a smaller amount of strain than was required to generate the same response in the quarter bridge circuit used for testing. The response of a quarter bridge circuit with a manufacturer-supplied gauge factor is given by equation 1.

$$\frac{V_0}{V_{ex}} = \frac{GF * \varepsilon}{4 + 2 * GF * \varepsilon}. \tag{1}$$

Equation 2 describes the voltage output of a full bridge circuit with each arm of the bridge instrumented with a piezoresistor.

$$\frac{V_{out}}{V_{in}} = GF * \varepsilon. \tag{2}$$

Using these equations, the strain required to achieve the necessary voltage threshold in the load cell is calculated to be nearly 1/4 of what is required in the experimental quarter-bridge circuit. Furthermore, the corresponding stress is calculated using the elastic modulus of the beam material, aluminum 6061-T6511. The result of this calculation served as a design constraint for subsequent FEA-based optimization.

For each design iteration, FEA determined the stress arising from the minimum expected load and revealed whether the measurement sensitivity was adequate to detect the smallest expected loads. Furthermore, FEA revealed the factor of safety present when subjected to the maximum expected load. Successive design iterations were modified by altering the size of the slots in the piezoresistor areas. The goal was to optimize the design to provide a good balance between the measurement sensitivity and safety factor. The length and shape of the slots were also gradually refined to provide an acceptably large area on which to mount the piezoresistors, while also meeting sensitivity and factor of safety constraints. The resulting design is shown in figure 7.

Figure 7. Resulting slotted design of load cell from FEA iterations.

6. Electrical Circuit Design

6.1 Gauge Placement

Proper operation of the full bridge measurement circuit requires the piezoresistors to be aligned with the strain fields so that the two branches of the circuit are adding their outputs and rejecting undesired modes of loading. This is accomplished by organizing the arms of the bridge as described in figure 8, with those labeled T and C subjected to tensile and compressive strains, respectively.

The output from the full bridge configuration used in figure 8 is given by equation 3 (*22*).

$$\frac{V_{out}}{V_{in}} = \left[\frac{R_3}{R_3 + R_4} - \frac{R_2}{R_1 + R_2} \right]. \tag{3}$$

In the case of lift and drag forces and moments, the beam is bent along one of its two longitudinal axes. As the load cell is bent, 1/2 of the beam will experience tension and the other half compression. By mounting the gauges according to figure 8, the output voltage for a given loading mode is seen, while the output from the undesired mode is rejected due to one arm of the measurement circuit exactly cancelling the other.

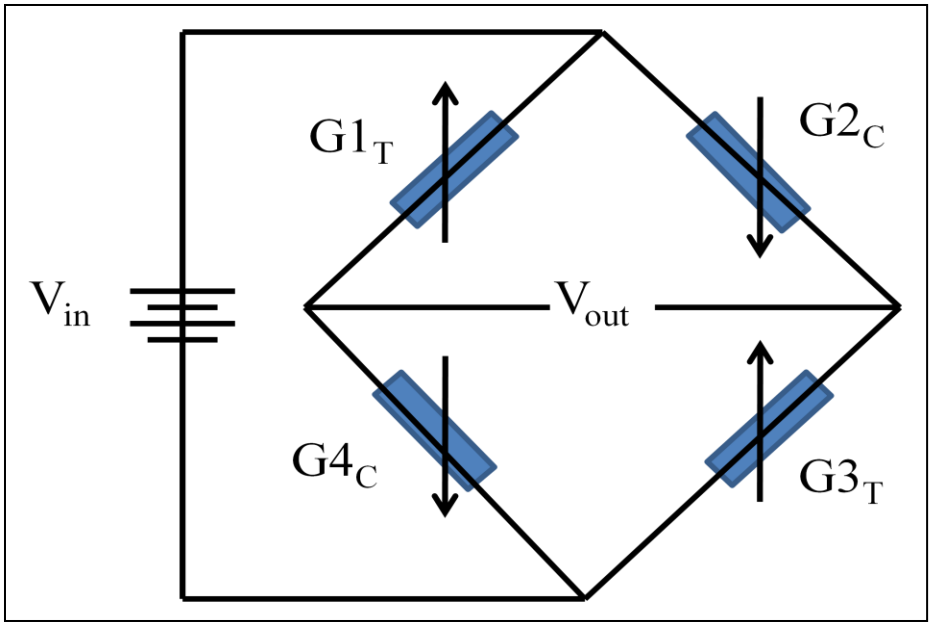

Figure 8. Standard full bridge configuration.

Figures 9–12 show the stress fields and corresponding gauge mounting locations for each of the three modes of loading to be measured. Lift and thrust are functionally equivalent, while axial torsion requires a different arrangement. However, it provides the same benefit of rejection of undesired modes of loading due to cancelling opposite arms of the circuit.

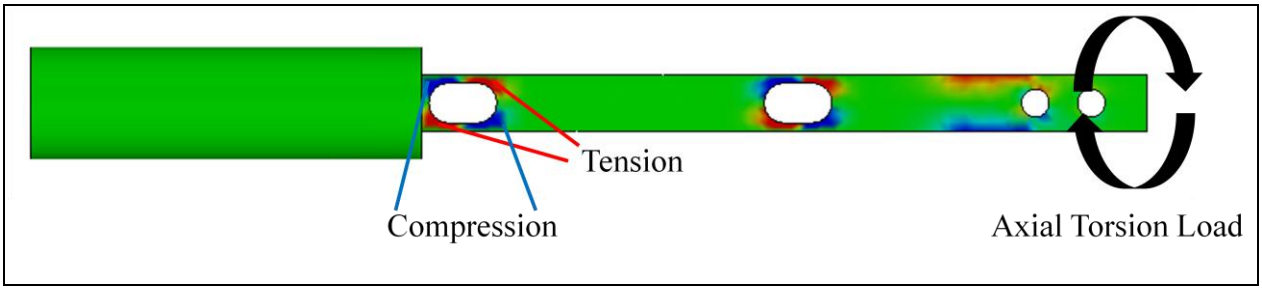

Figure 9. Bending/torsion loading modes and gauge placement.

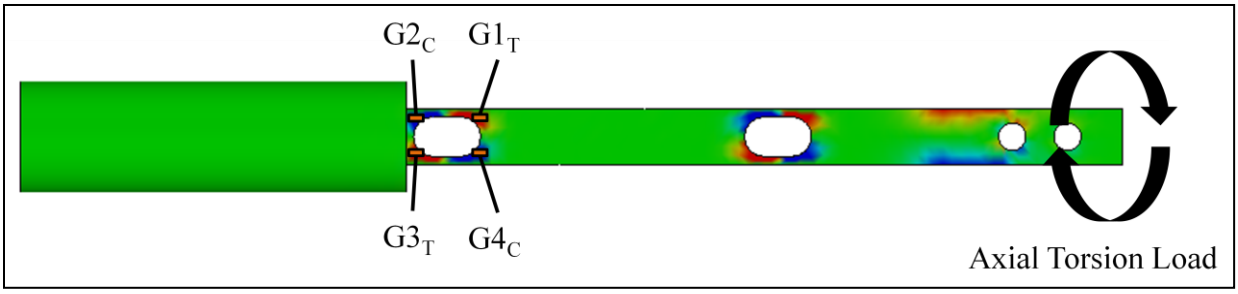

Figure 10. Bending/torsion loading modes and gauge placement.

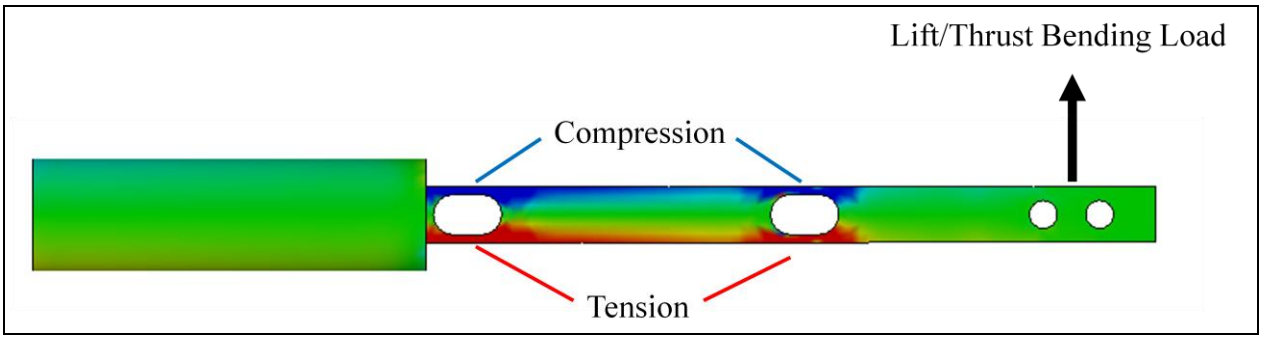

Figure 11. Bending/torsion loading modes and gauge placement.

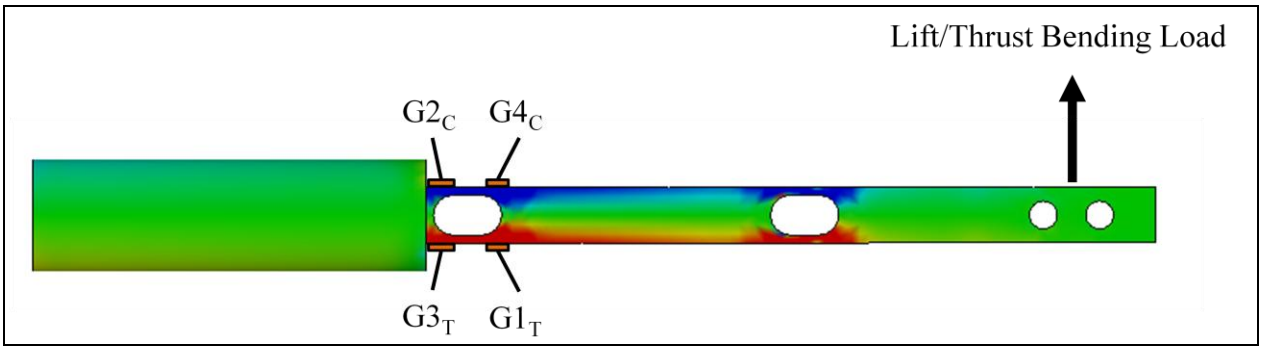

Figure 12. Bending/torsion loading modes and gauge placement.

6.2 Circuit Design Challenges

Piezoresistors have a number of challenges associated with their usage relative to traditional foil strain gauges. Temperature effects are important to account for due to changes in both resistance and gauge factor. Test environment variations over time and self-heating create thermal fluctuations that drive these changes. Self-heating occurs because as current flows through each piezoresistor, power is dissipated. The effect is more pronounced with larger excitation voltages, which are desirable due to improved output strength. Additionally, as the climate control systems function in the test environment, minor convection currents are expected to form in the oil tank due to the variation between the wall boundary layer and the interior oil. So even though

the gauges are to be used in a submerged environment, some degree of thermal variation can be expected during operation. To address these concerns, the bridge configuration shown in figure 13 is used for all measurement axes on the load cell.

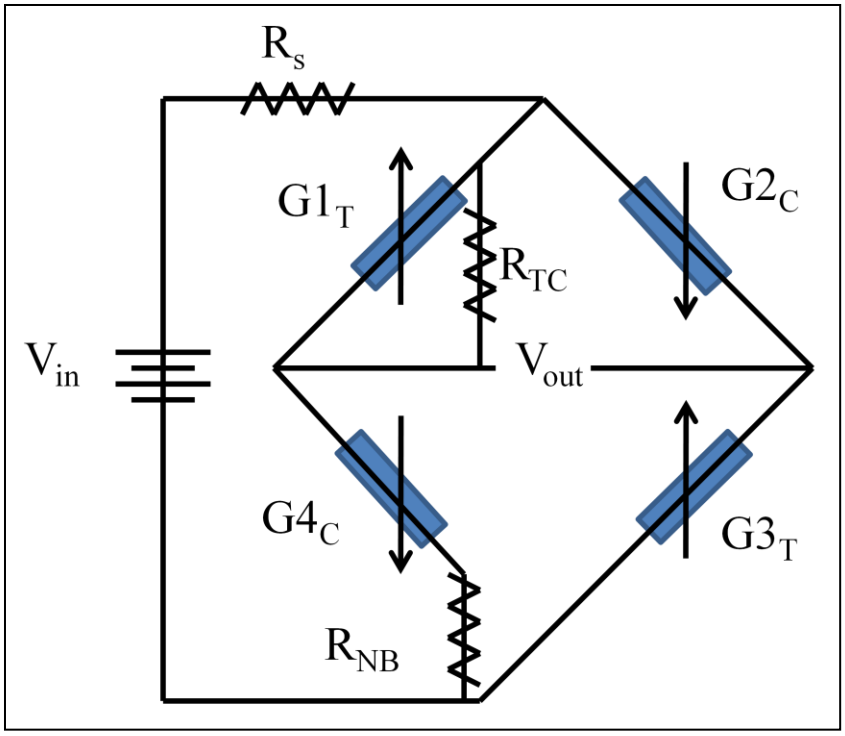

Figure 13. Modified bridge circuit with compensation.

The gauge factor of the piezoresistors in each of the four active arms is reduced as the temperature is increased because silicon has a large, positive temperature coefficient of resistance. This results in a reduction in apparent sensitivity ($\Delta R/R$) due to the large increase in resistance.

This circuit can be seen as a simple voltage divider, with the four active arms acting as one variable resistor in series with R_s and constant supply voltage V_{in}. The resistance of the four active arms will increase if exposed to temperature increases. Therefore, the voltage supplied to the active arms of the bridge will increase with temperature, thus boosting the output signal strength for a given strain. This effect can be exploited to compensate for the loss in sensitivity to the output signal caused by the reduction in gauge factor silicon experiences with elevated temperature.

Selection of the resistor in series with the power supply must properly balance the increased voltage to the active part of the circuit with the thermal reduction in-gauge factor. Proper resistance selection is described by equation 4 (*22*).

$$\frac{R_S}{R_B} = \frac{|F_{Tb}|}{\beta_b - |F_T|}. \quad (4)$$

R_s is the value of the resistor in series with the power supply, and R_B is the total bridge resistance as measured at the powered corners, effectively treating the active portion of the circuit as a single variable resistor. F_{Tb} is the bonded gauge temperature coefficient of gauge factor, and F_T is the unbonded gauge thermal coefficient of gauge factor; each is determined experimentally by the gauge manufacturer. β_b is the bonded gauge temperature coefficient of resistance, with behavior described by equation 5.

$$\beta_b = \beta + (\alpha_{s\_} \alpha_g) * F. \quad (5)$$

The first term β is the temperature coefficient of resistance of the unbonded gauge determined by the manufacturer using a series of thermal excursion tests over a range of interest for this application. The second term describes the differential expansion effect of temperature between the substrate material (α_s) and the gauge material (α_g), resulting in increasing levels of extensile stress as temperature is increased. F is the gauge factor.

The gauge R_{NB} at the bottom of the bridge acts as a precision zero-output nulling resistor and balances the bridge output to 0 V when the load cell is unloaded. This resistor is designed to correct small variations in the nominal resistance of each of the bridge circuit's arms. This resistor can be placed on either the left or right side of the bridge, with its ideal location and value determined for each individual bridge to precisely balance the output.

The gauge labeled R_{TC} is included in the circuit to prevent zero drifting due to thermal variations. This is different than the R_{NB} because that resistor is designed to zero the output when unloaded and at standard temperature. The ideal value and location of this resistor is experimentally determined by applying temperature excursions to each measurement circuit and determining the required value to balance the thermal effects. This resistor is placed to account for small differences in the thermal variability of each of the bridge circuit's arms.

7. Manufacturing and Installation

With the physical and electrical configurations determined, the next step was to determine the manufacturing and assembly procedure for the load cell. The piezoresistors require a number of challenging installation steps to ensure proper bonding to the beam. While it is possible to mount piezoresistors using two-part epoxy, significant degradation in performance results from small misalignments and bonding errors. Due to the very small size, it is challenging to avoid these errors. Therefore, the gauge handling and installation are left to the manufacturer due to the importance of proper alignment, positioning, and adhesion to the beam using a special type

of mounting cement and a precisely controlled heat treatment procedure. The piezoresistors are mounted to the surface of the load cell in the locations identified by the FEA performed.

The gauges are connected to solder pads mounted on the beam using 0.002-in-diameter gold wires to prevent stress from the weight of the wires affecting the measurements. Additionally, the gauges and wires are coated in a protective layer of room-temperature vulcanizing (RTV) rubber. Before completing the bridges and running the signal and power wires out of the bridge, the resistor matching steps described in section 6 must be performed. It is important to perform these steps at this time because small variations exist due to the mounting of each individual gauge. By accounting for this variability before completing each circuit, maximum accuracy and linearity are achieved.

Once the appropriate resistor values are selected to compensate for thermal sensitivity loss and zero drift, the bridges are completed. Next, the wires for power and signal need to be routed down the load cell and out of the oil tank. To accommodate these wires without blocking the motion of the flapping mechanism, four grooves are added to the clamped portion of the load cell. Once outside the oil tank, signal wires are routed into an amplifier and filter to provide increased signal strength and low-pass filtering. Finally, measurements are recorded using standard data acquisition software.

Previously, it was stated that aluminum was used to construct the load cell. Aluminum was chosen instead of steel for a number of reasons. Due to the lower elastic modulus, a given stress will result in greater strain response, thus increasing output from the bridge circuits. The balance is machined from aluminum 6061-T6511, with material properties listed in table 3. The T6511 temper is heat-treated for much greater yield strength than untreated 6061-O aluminum. While the overall strain at failure is decreased, this is irrelevant because any excursion into the plastic region would be considered a failure of the load cell. The increased yield strength allows improved measurement resolution by allowing a smaller cross section of material to be used. Therefore, greater strains are achievable before yielding failure occurs. Additionally, this grade of aluminum provides excellent machinability for easier manufacturing.

Table 3. Material properties of aluminum 6061-T6511.

Property	Value	Units
Elastic modulus	69	GPa
Poisson's ratio	0.33	—
Shear modulus	26	GPa
Density	2700	kg/m^3
Tensile strength	290	MPa
Yield strength	255	MPa

Machining consisted of first using a lathe to reduce a piece of larger round stock down to a 0.50-in diameter. Next, a combination of manual and computer numerically controlled milling operations was used to cut the aluminum to the proper dimensions. One additional feature added to the load cell was a chamfer at each end of the clamped end of the cylindrical portion to ease the installation process and reduce assembly stresses incurred from misalignment. The finalized part is shown in figure 14.

Figure 14. As-manufactured design of load cell.

8. Calibration

With the load cell installed in the flapping mechanism, the final step to prepare for testing was calibration. There were two primary goals to the calibration process. First, the coupling between measurement channels had to be determined. Second, the appropriate scaling factors had to be applied to measured voltages so that outputs were in the desired units.

Calibration was performed by generating a calibration matrix A, which related applied forces and moments x, to measured output voltages B, described by equation 6.

$$[A][x] = [B]. \tag{6}$$

The stiffness matrix was populated by applying a calibrated load to each of the axes of measurement. The coefficients relating output voltages to applied loads for each measurement channel were then recorded as rows of A, shown in table 4.

Table 4. Coefficients relating output voltages to applied loads recorded as A rows.

–103.3	0	58.39	0	0
0	–104.8	0	58.32	0
–43.27	–2.7	34.55	2.28	0
0	–42.89	0	33.79	0
0	0	0	0	73.44

The matrix A, when multiplied by an applied force, gives the measured output voltages. By inverting this matrix and multiplying by equation 6, any coupling between measurement channels is taken into account, and the measured voltages are related to forces experienced by the load cell.

$$[A]^{-1}[A][x] = [A]^{-1}[B]. \tag{7}$$

The modified equation states that the loads applied to the load cell during testing, *x*, will equal the inverted stiffness matrix, A^{-1}, times the measured voltages, *B*.

Examination of the calibration matrix revealed a few useful results. First, the large couplings in channels 1 and 3 and 2 and 4 are expected since these channels are resolving force and moment along the same axes described in section 4. Smaller magnitude off-axis coupling arising on measurement channel 3 is likely the result of the manufacturer's gauge placement process. The relative stiffness values show that the most sensitive axes are the two bending axes corresponding to lift and thrust. The torsion axis has about 71% the sensitivity of the lift and thrust axes, a result of the different gauge placement technique and load cell geometry.

9. Conclusions and Future Work

This load cell should prove to be a useful tool for measuring small forces and moments. The measurements can be taken with confidence because the load cell was designed, built, and calibrated with a single application in mind. Therefore, its properties are specifically tailored to match the expected loading conditions.

A benefit of this work has been the cost savings relative to the purchase of a similar commercially available load cell. A market survey of multiaxis load cells suitable for this application revealed two unfortunate realities. First, the range of commercially produced options at this size scale was quite limited. Second, those offered tended to be on the order of $10,000. This was one of the major motivating factors for undertaking the construction of this custom load cell.

The primary component of cost in this load cell was construction labor. This process included the preparation of the beam, application of gauges, curing of the epoxy, and thermal cycling to determine the required values of circuit completion resistors. This cost totalled under $3,000. The other main component of cost was the time spent designing and manufacturing the body of the load cell. This time would be comparable to the time required to design and build a custom wing mount that would be required if a commercially available load cell had been used. Therefore, the undertaking of a custom load cell design has yielded a cost savings of around 50%–75% over comparable commercially available products.

Moving forward, it is envisioned that this load cell will be used to measure the Reynolds scaled forces on a scaled fruit fly wing. The load cell will also be used to develop higher-performing wing designs in future tests, as well as to validate models of wing performance with experimental data.

10. References

1. Mastinu, G.; Gobbi, M.; Previati, G. A New Six-Axis Load Cell. Part I: Design. *J. of Exp. Mech.* **2011**, *51* (3), 373–388.
2. Carignan, F., et al. Force Measuring Platform and Load Cell Using Strain Gages to Measure Shear Forces. U.S. Patent 4,493,220, 1985.
3. Sheng, A. L.; Hung, L. T. A Novel Six-component Force Load Cell of Good Measurement Isotropy and Sensitivities. *Sensors and Actuators A*: *Physical* **2002**, *100* (2–3), 223–230.
4. Spletzer, B.; Marron, L. Information Package for the Simplified Six-Axis Load Cell. Sandia National Laboratories: Livermore, CA, January 2000.
5. Berme, N. Multi-component Force and Moment Measuring Platform and Load Transducer. U.S. Patent 6,354,155, 2002.
6. Blakeborough, A.; Clément, D.; Williams, M. S.; Woodward, N. Novel Load Cell for Measuring Axial Force, Shear Force, and Bending Movement in Large-scale Structural Experiments. *Exp. Mech.* **2002**, *42* (1), 115–122.
7. Gobbi, M.; Mastinu, G.; Giorgetta, F. Load Cells for Measuring Forces and Moments with Application to Ground Vehicle Design and Engineering. *Proceedings ASME IMECE*, paper n. IMECE2005-81143, 2005.
8. Nakamura, Y.; Yoshikawa, T.; Futamata, I. Design and Signal Processing of Six-Axis Force Load Cell. *Proc. of the 4th International Symposium of Robotics Research*, 1988; pp 75–81.
9. Bicchi, A. A Criterion for Optimal Design of Multi-axis Force Load Cells. *J. of Robotics and Autonomous Systems* **1992**, *10* (4), 269–286.
10. Svinin, M. M.; Uchiyama, M. Optimal Geometric Structures of Force/Torque Load Cells, *Inter. J. of Robotics Research* **1995**, *14*, 560–573.
11. Dickinson, M. H.; Lehmann, F.-O.; Sane, S. P. Wing Rotation and the Aerodynamic Basis of Insect Flight. *Science* **1999**, *284* (5422), 1954–1960.
12. Higdon; Ohlsen; Stiles; Weese; Riley. *Mechanics of Materials*; 3rd ed.; John Wiley & Sons, Inc.: New York, 1976.
13. Perry, C. C.; Lissner, H. R. *The Strain Gage Primer*; McGraw-Hill, Inc.: New York, 1962.
14. Sokolnikoff, I. S. *Tensor Analysis (Theory and Applications to Geometry and Mechanics of Continua)*; 2nd ed.; John Wiley & Sons: New York, 1964.

15. Hornsey; McFarland; Muhlbauer; Smith. *Mechanics of Materials (An Individualized Approach)*; Houghton Mifflin Company: Boston, 1977.

16. *Manual on Experimental Stress Analysis*; 3rd ed.; Society for Experimental Stress Analysis: Westport, CT, 1978.

17. Daily, J. W.; Riley, W. F. *Experimental Stress Analysis*; 2nd ed.; McGraw-Hill, Inc.: New York, 1978.

18. Murray, W. M.; Stein, P. K. *Strain Gage Techniques*; 1958.

19. Stein, P. K. *Advanced Strain Gage Techniques*; Stein Engineering Services, Inc.: Phoenix, AZ, 1962.

20. National Aerospace Standard 942, Revision 2. *Strain Gages, Bonded Resistance*; Aerospace Industries Association of America, Inc.: Washington, DC, 1 July 1964.

21. Hewlett-Packard Co. *Floating Measurements and Guarding*; Application Note 123; Hewlett-Packard Co.: Palo Alto, CA, 1970.

22. Sharpe, W., Ed. *Springer Handbook of Solid Mechanics*; Springer Science: New York, 2008.

NO. OF
COPIES ORGANIZATION

1 (PDF only) DEFENSE TECHNICAL INFORMATION CTR
DTIC OCA
8725 JOHN J KINGMAN RD
STE 0944
FORT BELVOIR VA 22060-6218

1 DIRECTOR
US ARMY RESEARCH LAB
IMNE ALC HRR
2800 POWDER MILL RD
ADELPHI MD 20783-1197

1 DIRECTOR
US ARMY RESEARCH LAB
RDRL CIO LL
2800 POWDER MILL RD
ADELPHI MD 20783-1197

1 DIRECTOR
US ARMY RESEARCH LAB
RDRL CIO MT
2800 POWDER MILL RD
ADELPHI MD 20783-1197

1 DIRECTOR
US ARMY RESEARCH LAB
RDRL D
2800 POWDER MILL RD
ADELPHI MD 20783-1197

NO. OF
COPIES ORGANIZATION

ABERDEEN PROVING GROUND

3 DIR USARL
RDRL VTA
A HARRINGTON
C KRONINGER
RDRL VTV
J GERDES